Smart Proof System Instructions

It is recommended that you read all instructions below; even if you are familiar with online review practices.

Using the Smart Proof system, proof reviewers can easily review the PDF proof, annotate corrections, respond to queries directly from the locally saved PDF proof, all of which are automatically submitted directly to **our database** without having to upload the annotated PDF.

- ✓ **Login into Smart Proof** anywhere you are connected to the internet.
- ✓ **Review the proof** on the following pages and mark corrections, changes, and query responses using the **Annotation Tools**.

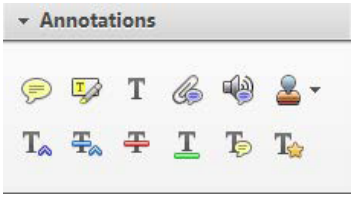

Note: Editing done by replacing the text on this PDF is not permitted with this application.

- ✓ **Save your proof corrections** by clicking the "Publish Comments" button.
  Corrections don't have to be marked in one sitting. You can publish comments and log back in at a later time to add and publish more comments before you click the "Complete Proof Review" button below.

- ✓ **Complete your review** after all corrections have been published to the server by clicking the "Complete Proof Review" button below.

Before completing your review.....

Did you reply to all author queries found in your proof?

Did you click the "Publish Comments" button to save all your corrections? Any unpublished comments will be lost.

Note: Once you click "Complete Proof Review" you will not be able to add or publish additional corrections.

Magnesium, aluminum, and zinc co-substituted hydroxyapatite: anti-corrosion properties

AQ:au

Lenka Šimková
Anorganická Technologie, Univerzita Pardubice, Pardubice, Czech Republic, and
Petra Šulcová
Univerzita Pardubice Fakulta Chemicko-Technologicka, Pardubice, Czech Republic

Abstract

AQ: 1

Purpose – The purpose of this study was to investigate the influence of doping ions Mg^{2+}, Zn^{2+}, Al^{3+} to the structure of hydroxyapatite (HAP; $Ca_{10}(PO_4)_6(OH)_2$) and subsequently to evaluate their adaptation in structure and their anticorrosive properties.

Design/methodology/approach – The substituted hydroxyapatite was synthesized by precipitation method that included the addition of Mg^{2+}, Zn^{2+} and Al^{3+} containing precursors to partially replace Ca^{2+} ions in the hydroxyapatite structure. For precipitation synthesis, three ratios of Ca/P = 1; 1.67; 3 and two values of pH = 7 and 12 were selected. Samples 1 (Ca/P = 1; pH = 7), 2 (Ca/P = 1.67; pH = 7), 3 (Ca/P = 3; pH = 7) and 5 (Ca/P = 1.67; pH = 12) were chosen to monitor the influence of doping ions Mg^{2+}, Zn^{2+} and Al^{3+} to the structure of hydroxyapatite and its anticorrosive properties.

Findings – The chosen synthesis conditions are appropriate for the formation of crystalline HAP substituted by elements Mg, Zn and Al. Only for one sample (1-Mg), two different phases (hydroxyapatite and whitlockite) were identified in the phase composition. On the basis of preliminary corrosion tests, pigments were divided into three groups pursuant to their anticorrosion effectivity: pigments with high corrosion-inhibition efficiency; pigments without anticorrosive properties; and pigments that promote corrosion processes.

Originality/value – In addition, no doping effect can be observed except for the sample 1-Mg, which consists of two phases (hydroxyapatite and whitlockite). Preliminary corrosion tests prove that some samples of HAP have extremely high anticorrosive effectivity as effectivity of the commercial pigments. The accelerated corrosion test showed that HAP samples have insufficient corrosion-inhibition properties for coating applications compared with the commercial pigment.

Keywords Corrosion, Inhibitors, Degradation, Corrosion science, Coatings and linings, Hydroxyapatite, Whitlockite, Co-substitution, Preliminary and accelerated corrosion tests, Corrosion

Paper type Research paper

1. Introduction

Pigments based on phosphorus compounds are currently the most significant group of pigments that have acquired the status of "non-toxic" anti-corrosion pigments (Buxbaum and Pfaff, 2005). Phosphates are used as an additive to the formulation of organic coatings of any type, providing easily available, cost-effective and metal protection against atmospheric corrosion. Like other inorganic salts, phosphates are kinetically active corrosion inhibitors that are essentially capable of affecting the rate of the corrosion process. The mechanism of phosphate inhibition consists a number of independent processes (Gorodylova *et al.*, 2016). Owing to the anionic part of phosphate inhibitors, these phosphate species are not themselves red-ox active and therefore are unable to initiate the formation of protective oxidized layers on the metal surface. This requires the contribution of other passivators (hydroxyl or oxygen groups present in the aqueous medium). In this case, a protective film consisting essentially of metal oxides or hydroxides is formed, while the phosphate anions steady and reinforce the protective oxide layer by the pore closing mechanism. Creating such an intensified passive layer in active corrosion zones reduces the rate of electrochemical reaction or blockades corrosion processes. The closing mechanism is considered to be the main subsidy to the inhibitory activity of phosphates. The occurrence of phosphates in the passive layer structure under the phosphate-containing paint was certified in few studies (Gorodylova *et al.*, 2016; Poledno, 2003). The cationic part of phosphate inhibitors, habitually alkaline earth metals, zinc, strontium and aluminum, does not have important inhibitory activity, nevertheless, it designates the relevant physicochemical properties of pigments such as their solubility and the pH of the environment. The low solubility of the pigment particles may initiate some anticorrosive species to participate in chemical corrosion inhibiting reactions. The pH of the environment influences the kinetics of corrosion reactions and the passivation of the produced product (Gorodylova *et al.*, 2016).

The current issue and full text archive of this journal is available on Emerald Insight at: **www.emeraldinsight.com/0003-5599.htm**

Anti-Corrosion Methods and Materials

[DOI 10.1108/ACMM-11-2018-2029]

This work has been supported by the IGU University of Pardubice (SGS_2018_007).

Received 8 November 2018
Accepted 22 February 2019

J_ID: ACMM ART NO: 10.1108/ACMM-11-2018-2029 Date: 29-June-19 Page: 2 Total Pages: 12 4/Color Figure(s) ARTTYPE="ResearchArticle"

In recent years, considerable attention has been paid to the use of hydroxyapatite (calcium hydroxyphosphate) in the field of orthopedics, where these phosphates have to replace either partially or completely bone tissue (Rivera-Muñoz, 2011; Gshalaev and Demirchan, 2013). Another application of apatite is its use as a protective coating of marble, adsorbent, and photocatalyst (Huang *et al.*, 2016a; Graziani *et al.*, 2016; Reddy *et al.*, 2007).

One of the most important requirements in using these apatite materials is that interactions that may exist in contact with living tissues are not toxic. As a result of friction and wear of HAP, it is necessary to study its mechanical and thermal behaviour. Some studies indicate that HAP stoichiometry plays an important role in mechanical properties. Better results provide a Ca/P ratio of between 1.60 and 1.67, and mechanical strength decreases when grain size exceeds 2 μm. For this reason, the importance of morphology and microstructure control during the synthesis of the HAP process is decisive (Rivera-Muñoz, 2011; Gshalaev and Demirchan, 2013). The structure of HAP can also accept minerals imitating bone material. The addition of biologically active ions to biochemical material based on HAP structure can increase the biological activity of implants. Especially because of its excellent cytocompatibility and osteoconductivity, synthetic hydroxyapatite has been extensively studied as a surface material for metallic implants. Hydroxyapatite containing minor groups and elements (e.g. CO_3^{2-}, HPO_4^{2-}, Na^+ and Mg^{2+}) as well as trace elements (e.g. Sr^{2+}, K^+, Cl^- and F^-); imitate bone mineral. These smaller groups and elements play an important role in the physiological reactions associated with bone metabolism (Huang *et al.*, 2016b).

The traditional choice of metals for implants has been limited to alloys with good biocompatibility and high corrosion resistance. For example, nowadays, alloys of magnesium, titanium, and zinc are used as an implant material. Magnesium and its alloys have importance for biomedical applications owing to their hopeful biocompatibility and degradability in living beings. In addition to biocompatibility, they have further advantages such as low density, high specific strength, high thermal conductivity and corresponding hardness (Mensah-Darkwa *et al.*, 2013). The use of magnesium as an implant material is restricted due to its fast corrosion in the occurrence of body fluids, which results in rapid release of undesirable corrosion products. This can lead to the production of gaseous hydrogen and alkalizing body fluid that can suppress wound healing and to necrosis of the ambient tissue. In small amounts, these corrosion products can be metabolized *in vivo* (Mensah-Darkwa *et al.*, 2013; Dunne *et al.*, 2016). To use magnesium as an effective implant, the range of magnesium rust must be decelerated. Surface coating materials that reduced corrosion rates and meliorate the mechanical and biological properties of magnesium and its alloys involve a HAP-based coating because its chemical and crystallographic structure is like to bone (Mensah-Darkwa *et al.*, 2013).

Very interesting is the substitution of Zn^{2+} ions to the structure of hydroxyapatite due to its occurrence in biological tissues and its multiple roles in biological functions. It has been demonstrated that involving Zn^{2+} ions into implants can support metabolism and bone growth, improve bone density and avert bone loss (Livitska *et al.*, 2016).

This work is focused on the influence of doping of Mg, Zn and Al elements to the structure of hydroxyapatite and subsequently to evaluate their adaptation in structure and their anticorrosive properties. Samples were prepared by the precipitation method. Three ratios of Ca/P = 1; 1.67 and 3 were selected; two pH ranges of 7 and 12, where ammonia hydroxide solution was used to adjust the pH; and precipitation rate of 2 ml/min. Based on the crystal size results from the previous study (Šimková *et al.*, 2018), when the SEM and XRD analysis proved the comparability between the minimum dimensions from the SEM images and the maximum dimensions from the XRD, samples 1 (Ca/P = 1; pH = 7), 2 (Ca/P = 1.67; pH = 7), 3 (Ca/P = 3; pH = 7) and 5 (Ca/P = 1.67; pH = 12) were selected for doping chosen ions (magnesium, zinc, and aluminum). The pigments were analyzed for particle size distribution, crystal size and morphology, phase composition and corrosion tests (preliminary and accelerated).

2. Experimental parts

2.1 Materials

$Ca(NO_3)_2{\cdot}4H_2O$ (98 per cent, Lachema, Czech Republic), $(NH_4)H_2PO_4$ (98 per cent, Lachema, Czech Republic), NH_4OH (25 per cent, Penta Chrudim, Czech Republic), $Al(NO_3)_3{\cdot}9H_2O$ (99.9 per cent, Sigma Aldrich, Germany), $Mg(NO_3)_2{\cdot}6H_2O$ (99 per cent, Lachner, Czech Republic), $Zn(NO_3)_2{\cdot}6H_2O$ (99 per cent, Lachema, Czech Republic) were used for precipitation method. For the synthesis of hydroxyapatite, solutions for starting materials ($Ca(NO_3)_2{\cdot}4H_2O$, $(NH_4)H_2PO_4$), $Al(NO_3)_3{\cdot}9H_2O$, $Mg(NO_3)_2{\cdot}6H_2O$ and $Zn(NO_3)_2{\cdot}6H_2O$ of 1 mol/l were prepared. The precise concentrations of these solutions were determined using analytical methods.

2.2 Chemical analysis of starting materials

Determination of calcium concentration was performed by a chelating method using Eriochrome black T as an indicator (Šimková *et al.*, 2018). Phosphorus concentration was resolved by the photometric method (Přibil, 1961). Magnesium and zinc concentration was decided by the chelating method using Eriochrome black T (Mg) and xylenol orange as an indicator (Přibil, 1961; Záruba, 2016). Determination of aluminum was performed by gravimetric method (Sommer, 1995).

2.3 Synthesis of HAP

To choose the appropriate synthesis conditions for the formation of doped HAP, thermodynamic stability of pure HAP phase in aqueous solution was analyzed and approved in laboratory conditions (Hermassi *et al.*, 2015). Figure 1 shows F1
the predominance area diagram for the Ca^{2+}-PO_4^{3-} water system at 25°C. It is obvious that hydroxyapatite is stable in the pH range from 4.8 to 14. Owing to this information, three Ca/P ratios were chosen for the synthesis of hydroxyapatite, which was studied at pH = 7 and pH = 12 based on the area of the hydroxyapatite form: AQ: 2

- Ca/P = 1. In this case, hydroxyapatite formation occurs in excess of phosphate ions.
- Ca/P = 1.67. This ratio corresponds to the Ca/P stoichiometry of hydroxyapatite.
- Ca/P = 3. Hydroxyapatite formation occurs in excess of calcium ions.

J_ID: ACMM ART NO: 10.1108/ACMM-11-2018-2029 Date: 29-June-19 Page: 3 Total Pages: 12 4/Color Figure(s) ARTTYPE="ResearchArticle"

Figure 1 Predominance area diagram for the Ca^{2+}- PO_4^{3-} system

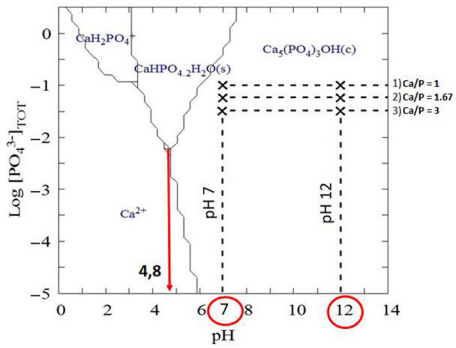

Samples 1 (Ca/P = 1; pH = 7), 2 (Ca/P = 1.67; pH = 7), 3 (Ca/P = 3; pH = 7) and 5 (Ca/P = 1.67; pH = 12) were selected for doping magnesium, zinc and aluminum ions. A total of 12 samples were prepared containing 0.5 mole of a substituted element under different synthesis conditions. Samples of the series 1 were substituted with Mg^{2+}, Zn^{2+} and Al^{3+} ions at the ratio (Ca + M)/P = 1 for M = Mg^{2+} and Zn^{2+} and 0.975 for M = Al^{3+} (precipitation rate of ammonium phosphate monohydrate 2 ml/min, pH = 7). Samples of the 2 series were replaced by Mg^{2+} and Zn^{2+} ions at a ratio of (Ca + M)/P = 1.67 and 1.625 for Al^{3+} ions (precipitation rate of ammonium phosphate monohydrate 2 ml/min, pH = 7). Samples of the series 3 were supplanted with Mg^{2+} and Zn^{2+} ions at a ratio (Ca + M)/P = 3 and 2.96 for Al^{3+} ions under the same precipitation conditions. In the case of samples 5, the ratio (Ca + M)/P = 1,67 for ions Mg^{2+} and Zn^{2+} and 1,625 for ions of Al^{3+} was chosen at the same precipitation rate but at different pH = 12.

The selected suitable precipitation conditions (Ca/P ratio; pH, precipitation speed) were adapted for the synthesis of doped HAP (Table I, precipitation speed 2 ml/min). For the synthesis of the samples, 1 M solutions of the starting compounds ($Ca(NO_3)_2{\cdot}4H_2O$, $Al(NO_3)_3{\cdot}9H_2O$, $Mg(NO_3)_2{\cdot}6H_2O$, $Zn(NO_3)_2{\cdot}6H_2O$, $(NH_4)H_2PO_4$) were prepared. The exact concentration of these solutions was determined using analytical

Table I Overview of the obtained samples and the synthesis conditions

Sample	Composition	(Ca+M)/P	pH
1	$Ca_{10}(PO_4)_6(OH)_2$	1	7
1-Mg	$Ca_{9.5}Mg_{0.5}(PO_4)_6(OH)_2$	1	7
1-Zn	$Ca_{9.5}Zn_{0.5}(PO_4)_6(OH)_2$	1	7
1-Al	$Ca_{9.25}Al_{0.5}(PO_4)_6(OH)_2$	0.975	7
2	$Ca_{10}(PO_4)_6(OH)_2$	1.67	7
2-Mg	$Ca_{9.5}Mg_{0.5}(PO_4)_6(OH)_2$	1.67	7
2-Zn	$Ca_{9.5}Zn_{0.5}(PO_4)_6(OH)_2$	1.67	7
2-Al	$Ca_{9.25}Al_{0.5}(PO_4)_6(OH)_2$	1.625	7
3	$Ca_{10}(PO_4)_6(OH)_2$	3	7
3-Mg	$Ca_{9.5}Mg_{0.5}(PO_4)_6(OH)_2$	3	7
3-Zn	$Ca_{9.5}Zn_{0.5}(PO_4)_6(OH)_2$	3	7
3-Al	$Ca_{9.25}Al_{0.5}(PO_4)_6(OH)_2$	2.96	7
5	$Ca_{10}(PO_4)_6(OH)_2$	1.67	12
5-Mg	$Ca_{9.5}Mg_{0.5}(PO_4)_6(OH)_2$	1.67	12
5-Zn	$Ca_{9.5}Zn_{0.5}(PO_4)_6(OH)_2$	1.67	12
5-Al	$Ca_{9.25}Al_{0.5}(PO_4)_6(OH)_2$	1.625	12

methods (titration, photometric and gravimetric analyses). The obtained precipitates were aged during 24 hours, filtered and washed with distilled water to neutral pH, then dried at 80°C for 6 hours (Figure 2). Analysis of the prepared samples was performed on an optical microscope (Dino-Lite Rack - MS 34 B, AnMo Electronics, Taiwan) directly after precipitation and in 2 and 24 h of aging. Particle size measurement was performed before and after aging (Mastersizer 2000 MU, Malvern Instruments Ltd., UK; Mie approach). The phase composition of the dried samples was analyzed on the benchtop X-ray diffraction instrument (Rigaku MiniFlex 600, Japan).

Preliminary and accelerated corrosion tests of the prepared powders were performed to verify their corrosion inhibition activity. Preliminary corrosion tests include the following: determination of pH and resistivity of aqueous suspensions of pigments (10 per cent), gravimetric determination of weight loss of steel plates, and determination of corrosion indicators for the steel plates after being dipped into pigment extracts for two months and the change of pH and resistivity during this process. The formed corrosion products were analyzed using optical microscope and their phase composition was determined by XRD analysis. Next, for accelerated corrosion tests, samples were dispersed in water-based primer paint and applied on steel substrates (approx. 22 × 5 × 0.1 cm) and tested in corrosion testing chambers (periodic wet-dry exposure to 100 per cent humidity with addition of 0.2 dm^3 of SO_2 gas at 38°C, Hydrotherm 519, Erichsen, Germany) during three weeks. The thickness of the dried paint coatings was controlled using a coating thickness gauge (Surfix easy I-FN, Phynix, Germany). The color change of the paint samples during the corrosion tests was measured using spectrophotometer (ColorQuest XE, HunterLab, USA). The evaluation of the degradation of the coatings was carried out with respect to the degree of rusting, blistering, cracking, flacking, and delamination according to ISO standards. Evaluation of the degree of corrosion on steel surface was carried out after removal of the paint using NaOH solution (30 Wt.%). Corrosion defects were also analyzed using an optical microscope. The commercial pigments ZP-10 (mixture $Zn_3(PO_4)_2{\cdot}2H_2O$ and $Zn_3(PO_4)_2{\cdot}4H_2O$; Heubach, Germany) and Zp-Bs-M (mixture $Zn_3(PO_4)_2{\cdot}2H_2O$ and ZnO; France) were tested in parallel with the synthesized samples.

2.4 Characterization of hydroxyapatite

The size of the crystals can be measured and characterized by optical microscope and the crystallinity and phase composition of the synthesized powders can be characterized by XRD.

2.4.1 Optical microscope (OM)

The dimension of the crystals was studied by digital optical microscope with magnification 10×-70× and 200×.

2.4.2 Measuring of particle size distribution

The particle size distribution of the synthesized powders was measured using an equipment Mastersizer 2000/MU. This device provides volumetric distribution and uses the laser diffraction on particles dispersed in a liquid medium. The particle size distribution was analyzed by two lasers – blue light (laser diode with wavelength 466 nm) and red light (He–Ne laser with wavelength 633 nm). The pigments were ultrasonically (Bandelin, Germany) homogenized in the solution of $Na_4P_2O_7$ (c = 0.15 mol/dm^3) for 2 min. The signal was evaluated on the

J_ID: ACMM ART NO: 10.1108/ACMM-11-2018-2029 Date: 29-June-19 Page: 4 Total Pages: 12 4/Color Figure(s) ARTTYPE="ResearchArticle"

Figure 2 Flow chart for the synthesis of HAP by precipitation process

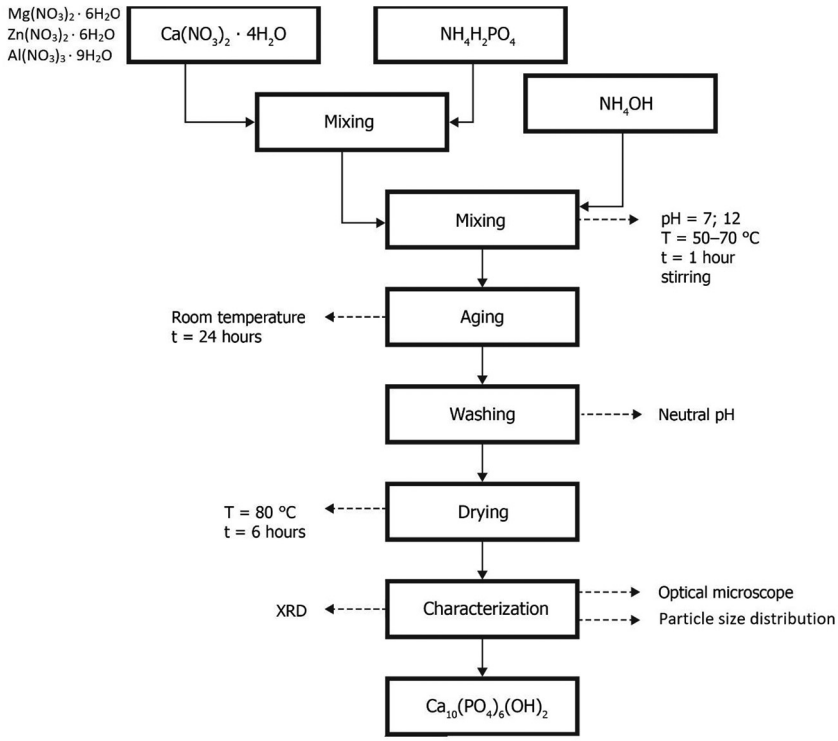

basis of Mie scattering. The measurement is taken in three steps, and results are automatically calculated as average and presented as d_{10}, d_{50} and d_{90} values.

2.4.3 X-ray diffraction analysis

The phase analysis of the powdered materials was studied by X-ray diffraction analysis (XRD). The phase composition was determined using diffractometer MiniFlex 600 with a vertical goniometer of 17 cm in the 2θ range of 10°–50°. The accuracy of goniometer was ±0.02°. X-ray tube with Cu anode (U = 40 kV, I = 15 mA) was used (CuKα radiation).

3. Results and discussion

3.1 Optical microscope

All prepared powders, in which a portion of Ca^{2+} ions was substituted by Mg^{2+}, Zn^{2+} or Al^{3+} ions, were studied by the digital optical microscope. To monitor how the morphology of the samples changed because of aging, the samples were measured immediately after precipitation (Figure 3a) and 24 h after aging (Figure 3b). F3

According to optical microscopy results, the doped HAP formed as agglomerates of small crystallites of different size and

Figure 3 The standard appearance of samples 1-Mg, 1-Zn and 1-Al (ratio Ca/P = 1; pH = 7; 2 ml/min) measured directly after precipitation (a) and after 24 h aging (b)

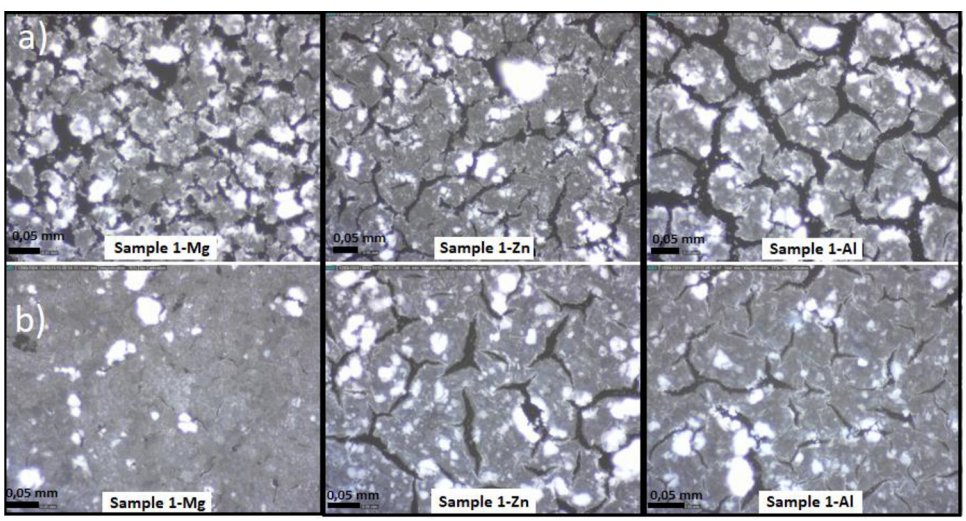

J_ID: ACMM ART NO: 10.1108/ACMM-11-2018-2029 Date: 29-June-19 Page: 5 Total Pages: 12 4/Color Figure(s) ARTTYPE="ResearchArticle"

shape similar to the pure HAP samples. Owing to the very small percentage of the content of doped elements, it was assumed that the size and shape of crystallites of doped samples are similar to not modified HAP. In particular, under the chosen conditions, HAP phase forms as nanocrystalline which size and shape depend on the Ca/P ratio (with Ca/P = 1 form need-like crystallites, with Ca/P = 1.67 – thin plates, with Ca/P = 3 – needle-like, thin plates and bulk crystallites), pH (with pH = 7 from larger and thinner crystallites, with pH = 12 - smaller and bulk crystallites), does not depend on the precipitation speed. Particle size measurements of the samples showed the values of d_{50} in ranged from 13.18 to 20.42 μm. These values indicate the size of agglomerates, which are slightly larger than the values for not-doped HAP samples.

3.2 Particle size distribution

Particle size distribution of synthesized samples was measured after 24 h aging with the Mastersizer 2000 MU. Signal was evaluated by Mie scattering. The distribution curves and d_{10}, F4 d_{50}, d_{90} and distribution span were obtained. Figure 4 shows the summary of volume distribution curves of unmodified and doped samples 1, 2, 3 and 5.

From the distribution curves of sample 1 (Figure 4a), it is clear that the sample of unmodified hydroxyapatite has a distribution curve shifted to lower values compared to modified HAP. The highest mean value of d_{50} showed a sample of T2 hydroxyapatite substituted with Mg^{2+} ions (Table II). For sample 2 (Figure 4b), it is clear that the sample of pure HAP has the lowest particle size values. The mean particle size d_{50} is less than 10 μm, while the Mg^{2+}, Zn^{2+} and Al^{3+} ions lead to an increase in d_{50} to 10-20 μm. The distribution curves for samples 3 (Figure 4c) are almost comparable, however, the modified Zn^{2+} ions exhibit the highest d_{50} value (Table II). Samples 5 provide significantly wider distribution curves (Figure 4d). The pure hydroxyapatite of sample 5 gave the lowest d_{50} value and also the lowest distribution width. In contrast, the highest d_{50} value, as well as the d_{10} and d_{90} values, was measured at the sample containing the Al^{3+} ions. Table II also shows that, in the case of samples substituted Mg^{2+} ions, there is a context between the ratio (Ca + M)/P and the mean particle size values, respectively agglomerates. If the ratio increases, the mean values are reduced.

Table II Particle size distribution of all synthesized samples

Sample	d_{10} [μm]	d_{50} [μm]	d_{90} [μm]	Span
Particle size distribution				
1-Mg	13.72	25.15	44.67	1.23
1-Zn	5.61	14.25	29.27	1.66
1-Al	7.62	15.89	28.97	1.34
2-Mg	7.50	16.09	29.98	1.40
2-Zn	6.53	14.04	26.07	1.39
2-Al	7.51	17.49	38.37	1.76
3-Mg	4.96	11.67	23.49	1.59
3-Zn	8.49	17.24	32.26	1.38
3-Al	4.86	13.18	29.09	1.84
5-Mg	6.55	15.56	45.73	2.52
5-Zn	6.41	15.70	42.01	2.27
5-Al	9.48	20.42	54.01	2.18

Figure 4 Distribution curves of doped samples 1, 2, 3 and 5

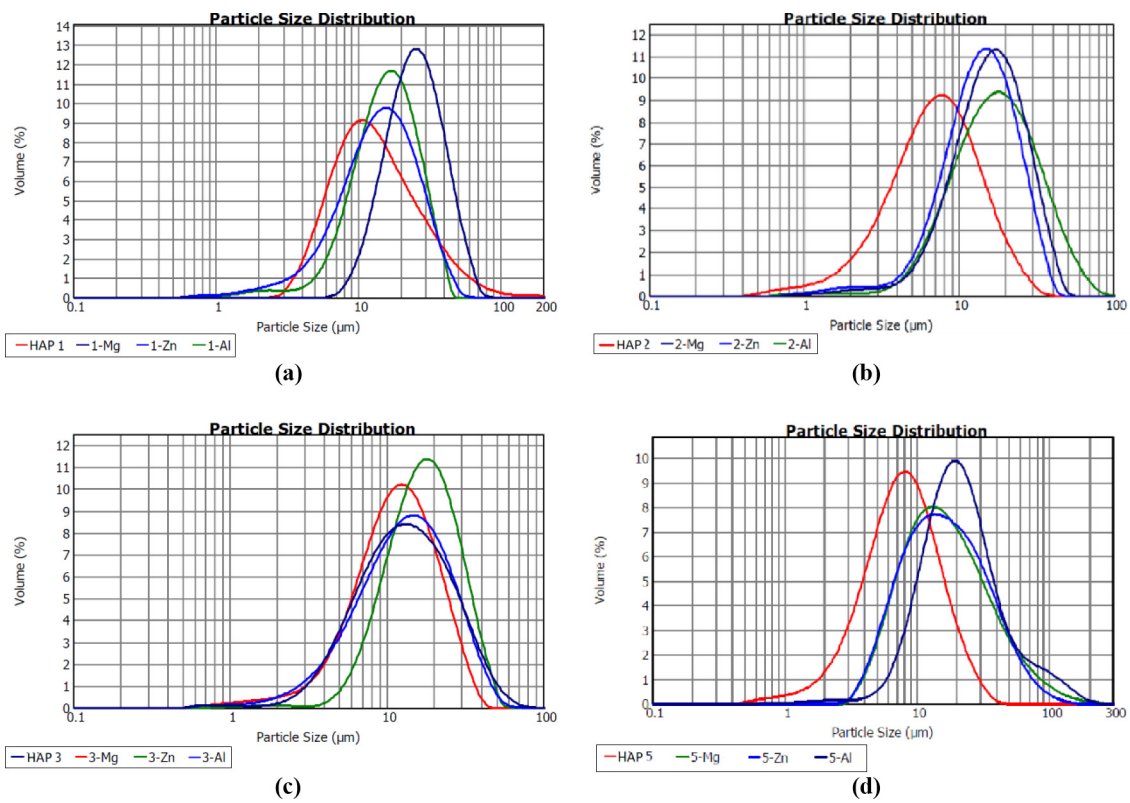

J_ID: ACMM ART NO: 10.1108/ACMM-11-2018-2029 Date: 29-June-19 Page: 6 Total Pages: 12 4/Color Figure(s) ARTTYPE="ResearchArticle"

3.3 X-ray diffraction analysis

The phase composition of the samples was determined by XRD analysis. According to XRD analysis, most samples showed a single phase composition of HAP (hexagonal or monoclinic F5 $Ca_{10}(PO_4)_6(OH)_2$, Figure 5). Only one sample – 1-Mg – consists of two phases: hydroxyapatite $Ca_{10}(PO_4)_6(OH)_2$ with the parameters: monoclinic crystalline system; spatial group $P2_1/b$ and whitlockite $Ca_{18}Mg_2H_2(PO_4)_{14}$ with parameters: F6 rhombohedral crystalline system; space group R_3C (Figure 6). Because only the HAP phase has been identified in other doped samples, it is clear that doping elements Mg, Zn, and Al occupy the calcium positions in the crystal structure of HAP. This can be expected because the atom radius of these elements are approximately same to or smaller than the radius of Ca (r (Ca^{2+}) = 0.106 nm (c.n.7), r (Mg^{2+}) = 0.089 nm (c.n. 8), r (Zn^{2+}) = 0.09 nm (c.n. 8), r (Al^{3+}) = 0.0535 nm (c.n. 6)).

The crystal size was calculated from the diffractogram based on the diffraction line width using the Scherrer equation, Williamson–Hall (WH) (Kalita and Kalita, 2017) and the Halder–Wagner (HW) method (Motevalizadeh *et al.*, 2014). Based on the XRD patterns, i.e. XRD reflection width, the crystallite size of the powders was also calculated (Table III). T3 The size of the crystallites of doped HAP is in the range of 2.81-49.2 nm according to the results based on Scherrer equation, 5.3-7.1 nm – the Hall–Wagner method, and 5.9-10.6 nm – the Williamson–Hall method. The large difference in crystallite size which was calculated according to the Scherrer equation can be explained by the large difference of the crystal dimensions. In

Figure 5 (a) Diffractogram of sample 1 (hexagonal HAP); (b) diffractogram of sample 2 (monoclinic HAP)

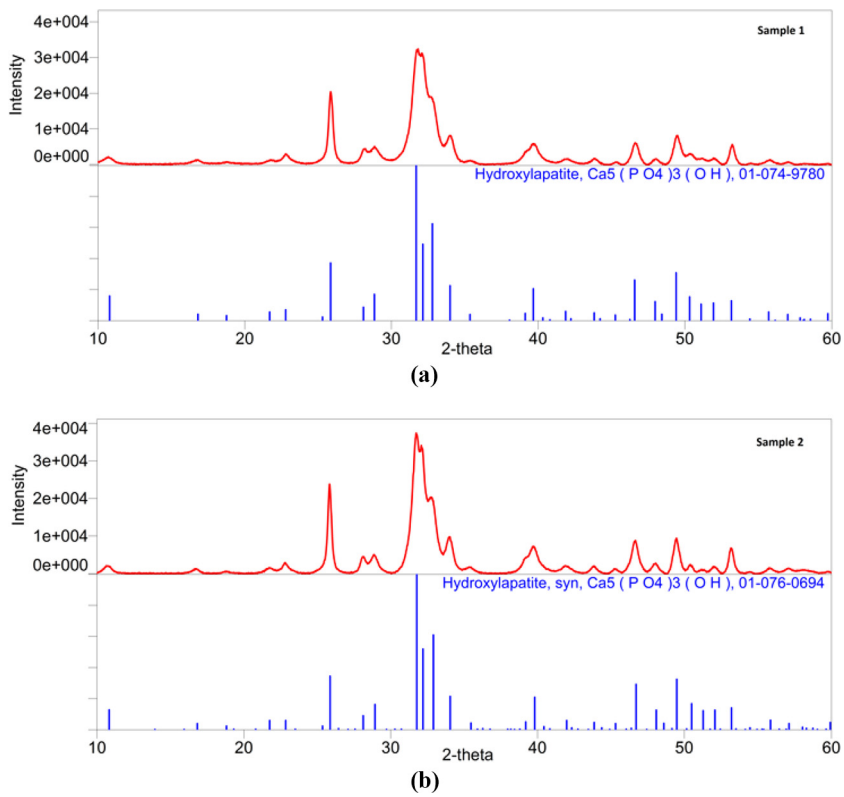

Figure 6 The diffraction pattern of the sample 1-Mg

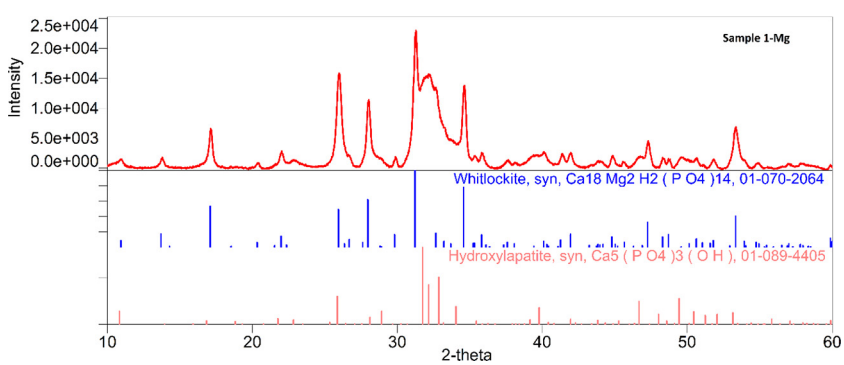

J_ID: ACMM ART NO: 10.1108/ACMM-11-2018-2029 Date: 29-June-19 Page: 7 Total Pages: 12 4/Color Figure(s) ARTTYPE="ResearchArticle"

Table III Crystallite size of synthesized hydroxyapatite samples

Sample of HAP	Crystallite size according to Sherry's equation Crystallite size [nm]	Crystallite size according to H–W method Crystallite size [nm]	Crystallite size according to Hall method Crystallite size [nm]
1-Mg	3.81-49.2	5.38 (1)	10.6 (6.1)
1-Zn	2.82-23.57	7.1 (1.1)	10.5 (7.4)
1-Al	5.11-19.4	5.3 (0.9)	6.3 (2.2)
2-Mg	3.5-19.2	6.58 (1.2)	5.6 (1.1)
2-Zn	3.4-16.7	5.0 (0.4)	5.5 (1.8)
2-Al	4.14-20.5	7.3 (0.9)	7.3 (2.7)
3-Mg	4.15-21.4	6.74 (1.8)	7.9 (2.5)
3-Zn	3.55-15.2	6.2 (0.7)	5.7 (1.8)
3-Al	3.49-24.9	6.3 (0.4)	7.2 (2.3)
5-Mg	3.2-18.7	6.2 (0.4)	5.9 (1.8)
5-Zn	4.5-16.2	6.0 (0.4)	7.8 (2.9)
5-Al	4.0-17.0	6.3 (0.5)	6.9 (1.5)

general, crystallites of doped samples are slightly smaller than for pure HAP.

3.4 Corrosion tests

3.4.1 Preliminary corrosion test

Preliminary corrosion tests do not evaluate visible changes in samples that have resulted from a corrosion test, but the value associated with the process of degradation of organic coatings is measured. These tests include determination of pH and resistivity of aqueous suspensions of pigments (10 per cent), gravimetric determination of weight loss of steel plates, and determination of corrosion indicators for the steel plates (Myšková, 2014; Mojžíš, 1967). Measurement of pH and resistivity of aqueous suspensions of pigments is intended to analyze the corrosive environment of pigments. The pH value in the range 7-9 is generally considered to be optimal for the best performance of anticorrosion pigments. Phosphate anticorrosion pigments show high efficiency in a slightly acidic pH range. Resistivity is an indicator of the concentration of dissociated ions in suspension, which are formed in result of the hydrolysis of pigment and may participate in the corrosion inhibition processes. This means that the resistivity of the aqueous pigment suspensions is an indicator of the solubility of the pigment in water. The partial solubility of pigment particles is very important for the effectiveness of anticorrosive phosphate pigments. Figure 7 shows change of pH and conductivity of the pigment suspensions during 28 days.

The measured values present that the hydrolysis of the pigment ions supports the formation of acid species, leading to decrease of pH. The conductivity of the samples was very different, but in general, it increased indicating that the concentration of dissociated ions has increased over time. The aqueous suspensions of the pigments were filtered and the pigments extracts were used for the assessment of weight loss of steel plates, which were submerged to extracts for three months. During the test, a different color change of the extracts was observed because of the release of corrosion products (Figure 8). At the same time, the significant increase in pH also indicated intense corrosive processes (cathodic

Figure 7 Results of preliminary corrosion tests: change of the pH and conductivity of the pigment suspensions during 28 days of aging

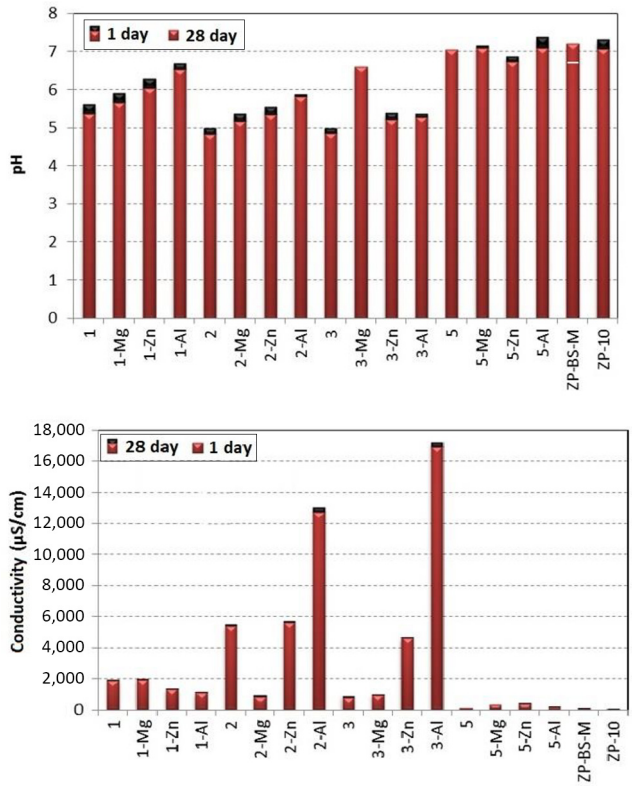

reaction leads to release of hydroxyl species: $O_2 + 2H_2O + 4e^- \rightarrow 4OH^-$). However, for all samples, the conductivity value reduced. This means that the dissociated ions from the pigment extract have been involved in the formation of a protective layer on the steel surface or other solid products.

Next, corrosion indicators were calculated on basis of corrosion losses of steel plates. Figure 9 shows a relative corrosive decrease for all tested samples. In this case, the water loss is a standard appropriate to 100 per cent.

On basis of the performed tests, the samples can be divided into 3 groups according to their anticorrosion efficiency.

First group – pigments with high anticorrosive efficiency: Corrosion processes in the pigment extracts have been decelerated owing to sufficient concentration of phosphates that inhibit corrosion processes (supported by the mild conductivity values and the formation of Vivianite $Fe_3(PO_4)_2 \cdot 8H_2O$ on steel surface). A sample of 1-Mg ($Ca_{9.5}Mg_{0.5}(PO_4)_6(OH)_2$) from this group demonstrated the best anticorrosive properties, which may be related to phase composition (Whitlockite phase may be more effective for corrosion protection than hydroxyapatite). This group contains mainly of the samples of series 1 which are formed of crystallites of the needle-like shape of the smallest size.

The second group – pigments without anticorrosive properties: The concentration of phosphate in these extracts is deficient for high anticorrosion efficiency (supported by low conductivity values and formation of FeO(OH) as the main corrosion product). This group includes the samples of series 5.

The third group – pigments that support corrosion processes: In this case, the corrosion processes were very intensive because of

Figure 8 The color change of the extracts owing to the release of corrosion products during 3 month of aging

Sample		1	1-Mg	1-Zn	1-Al	2	2-Mg	2-Zn	2-Al	3	3-Mg	3-Zn	3-Al	5	5-Mg	5-Zn	5-Al	H_2O	ZP-10	ZP-BS
Synth. cond.		Ca/P = 1 pH = 7				Ca/ P = 1.67 pH = 7				Ca/P3.16 pH = 7				Ca/P1.67 pH = 12					Comm. pigm.	
Before	σ [μS/cm]	2020	2070	1367	1082	5590	1035	5850	13330	997	1079	4910	17600	145	352	442	200	12.5	333	138
	pH	5.4	5.67	6.09	6.52	4.97	5.17	5.32	5.74	4.96	6.23	5.21	5.4	6.87	6.76	6.53	6.9	6.77	6.12	6.57
After immersion of steel plates	7 days																			
	3 months	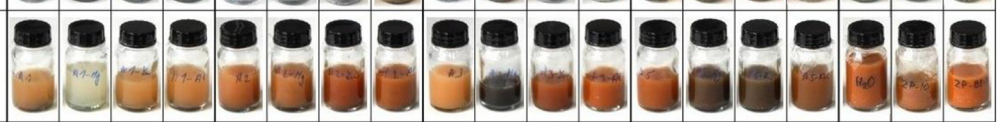																		
After	σ [μS/cm]	1430	1940	1367	693	4450	580	4800	12170	312	360	3570	15500	111	272	268	157	29	120	119
	pH	8.55	6.66	8.56	8.63	8.62	8.23	8.58	8.64	8.45	9.04	8.46	8.77	8.26	7.92	8.62	7.84	8.26	6.85	7.64

F10 **Figure 9** Results of the preliminary corrosion tests: relative decrease of weight of the samples (water – 100%)

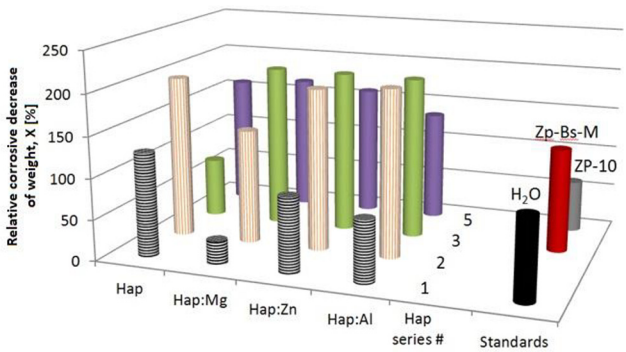

the intensive reaction between the pigment extracts and the steel plate (supported by the very high conductivity values, substantial surface corruption and the formation of FeO(OH)). Such behaviour can be explained by the occurrence of some hydrated complexes of calcium or doping elements, which operate as catalysts for corrosion. This group incorporates the samples of series 2 and 3.

3.4.2 Accelerated corrosion test

Accelerated laboratory tests expedite the corrosion processes on the exposed samples, resulting in rapid corrosion changes on the metal substrate as well as on the organic coating. For the accelerated corrosion tests, samples 1, 1-Mg, 1-Zn, 2, 3, 5 and ZP-10 were selected. These selected pigments were dispersed in the alkyd primer paint. The change in the appearance of the corrosion coatings was obvious visually. The images of all selected samples after the corrosion test are demonstrated in Figure 10. Some samples showed visually more yellow corrosion products (samples 2 and 3), some less (sample 1, 1-Mg, 1-Zn, 1-Al, 5) and the best visual appearance showed a commercial pigment (ZP-10). However, these coloring may be induced by diffusion of corrosion products from the edges of steel sheets, with corrosive stains being very visible.

Examples of coating degradation for the selected samples are revealed in Figure 11. The assessment of the degradation of the F11 coatings after the accelerated corrosion test showed that under the given conditions, the best corrosion properties exhibit sample 5 and the worst is sample 3. The least damaged sample is the ZP-10 (commercial pigment). This result consents with the color change of the samples where for the most damaged sample was determined the highest color difference. For all tested HAP samples, the formation of small crystals on the coating surface was observed (Figure 11). XRD analysis of these crystals identified only organic compounds in their phase composition, which suggests the destruction of the coating. Therefore, based on the accelerated corrosion test, HAP samples showed insufficient corrosion properties for coating applications in collation to standard pigment (ZP-10).

The evaluation of the degradation of the coatings after the accelerated corrosion test was performed with respect to the degree of rusting, blistering, cracking and flacking. Evaluation of the degree of delamination and corrosion in the vicinity of the cut and on the surface was executed after elimination of the coating. All results are shown in Table IV. The appearance of T4 the surface of the steel sheets after paint removal is demonstrated in Figure 12. The evaluation of paint F12 degradation and corrosion on the steel surface was made according to international norms (ČSN ISO 8407, 1995; ČSN ISO 6270-1, 2002; ČSN ISO 3231, 1998; ČSN ISO 4628-1, 2004; ČSN ISO 4628-2, 2004; ČSN ISO 4628-3, 2004;

Figure 10 Appearance of coatings after accelerated corrosion test

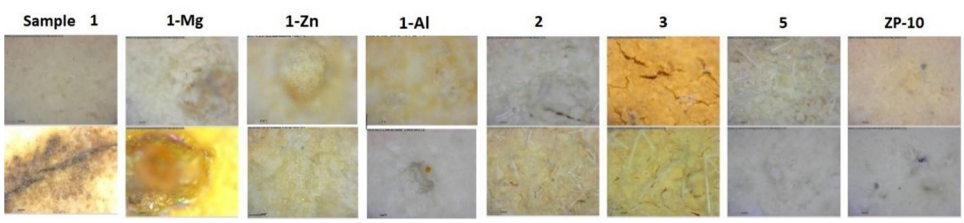

J_ID: ACMM ART NO: 10.1108/ACMM-11-2018-2029 Date: 29-June-19 Page: 9 Total Pages: 12 4/Color Figure(s) ARTTYPE="ResearchArticle"

Figure 11 Appearance of steel sheets of all tested samples after an accelerated corrosion test

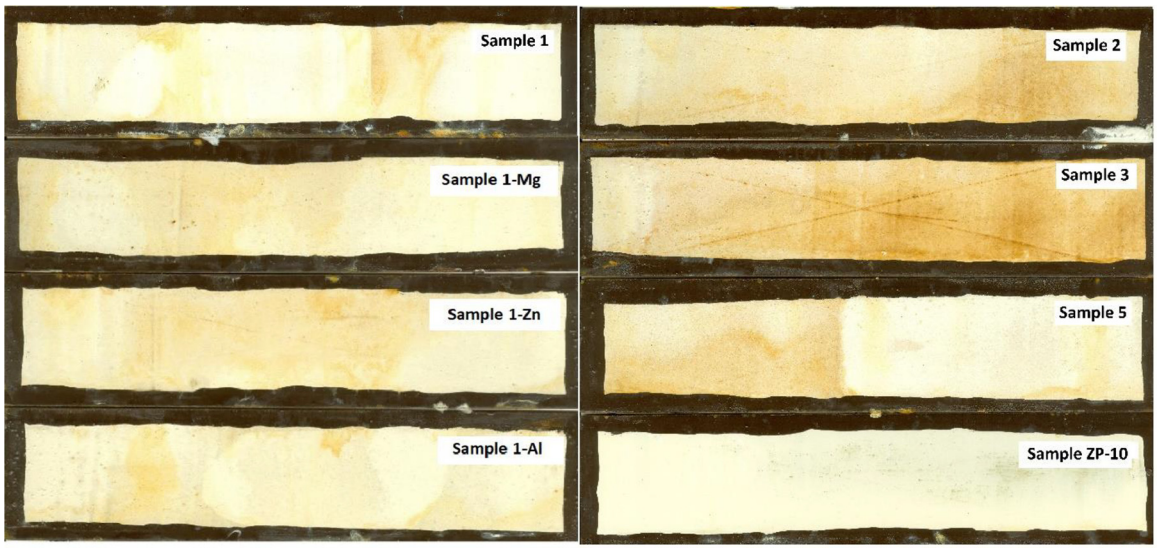

Table IV Evaluation of paint degradation

Sample	Rusting [%]	Blistering (quantity and size)	Cracking (classification and quantity)	Corrosion of steel In the vicinity of the cut [mm]	Corrosion of steel On the surface [%]
1	0.05	–	3;1	1	90
1-Mg	0.5	–	3;1	1	90
1-Zn	0.05	2-2(S4)	1;-	1	90
1-Al	0.05	2-2(S4)	1;-	1	80
2	0.5	–	1;-	1	85
3	1-2	2-2(S3)	3;2	1	75
5	0.05	–	1;-	1	90
ZP-10	0	–	-;-	–	30

ČSN ISO 4628-4, 2004; ČSN ISO 4628-5, 2004; ČSN ISO 4628-8, 2005). The rusting was evaluated as a percentage of rust. The quantity (density) and size of blistering were assessed using image standards. Classification and density of cracking were judged using image standards. The appraisal of the degree of corrosion in the vicinity of the cut was evaluated as the width of the corrosion products. The surface corrosion was evaluated as a percentage of the corroded area to the whole area.

In general, the lowest degree of rusting, blistering, cracking and corrosion was observed for sample ZP-10. The results show that under the given conditions sample 5 proves better corrosion properties and sample 3 the worst corrosion properties. The wicked corrosion properties of sample 3 in the accelerated corrosion tests consent with the results of the change in appearance of the paint and preliminary corrosion tests. For other samples, there is no context between the result of preliminary and accelerated corrosion tests.

AQ: 3

4. Conclusions

On basis of the obtained results, it can be concluded that the chosen synthesis conditions are appropriate for the formation

Figure 12 Appearance of samples after paint removal

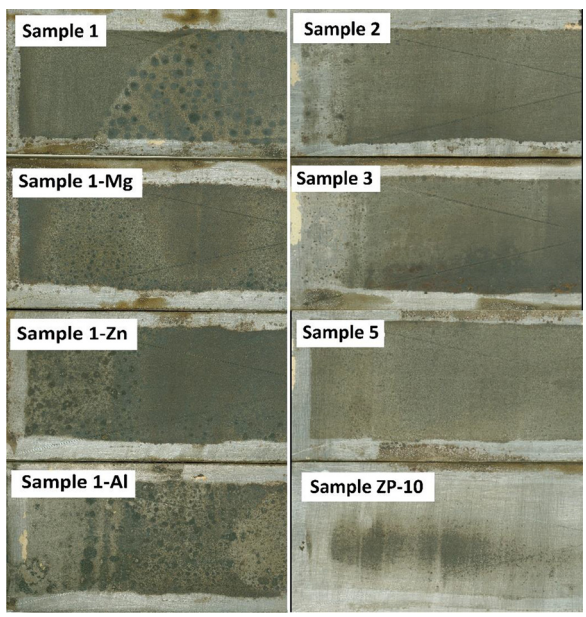

of crystalline HAP substituted by elements Mg, Zn and Al. Only for one sample (1-Mg), two different phases (hydroxyapatite and whitlockite) were identified in the phase composition. Therefore, in other cases, the elements occupy the positions of calcium in the crystal structure of HAP. On basis of preliminary corrosion tests, pigments were divided into 3 groups pursuant to their anticorrosion effectivity: pigments with high corrosion inhibition efficiency; pigments without anticorrosive properties; pigments that promote corrosion processes. It was also shown that the anti-corrosion efficiency of the prepared samples is connected with precipitation conditions. The best anticorrosion efficiency demonstrates the samples of needle-like crystallites of smallest size (series 1). In addition, no doping effect can be observed except for the

J_ID: ACMM ART NO: 10.1108/ACMM-11-2018-2029 Date: 29-June-19 Page: 10 Total Pages: 12 4/Color Figure(s) ARTTYPE="ResearchArticle"

sample 1-Mg, which consists of two phases (hydroxyapatite and whitlockite). Preliminary corrosion tests prove that some samples of HAP have very high anticorrosive effectivity as effectivity of the commercial pigments. The accelerated corrosion test showed that HAP samples have insufficient corrosion inhibition properties for coating applications compared to the commercial pigment. The poor corrosion properties of the pigments in the coating may be related to their low compatibility with the coating, which could be solved by surface modification of the pigment.

References

Buxbaum, G. and Pfaff, G. (2005), *Industrial Inorganic Pigments*, 3th ed., WILEY-VCH Verlag GmbH & Co, Weinheim.

ČSN EN ISO 3231 (67 3096) (1998), Nátěrové hmoty - Stanovení odolnosti vlhkým atmosférám s obsahem oxidu siřičitého.

ČSN EN ISO 4628-1 (67 3071) (2004), Nátěrové hmoty - Hodnocení degradace nátěrů - Klasifikace množství a velikosti defektů a intenzity jednotných změn vzhledu - Část 1: Obecný úvod a systém označování

ČSN EN ISO 4628-2 (67 3071) (2004), Nátěrové hmoty - Hodnocení degradace nátěrů - Klasifikace množství a velikosti defektů a intenzity jednotných změn vzhledu - Část 2: Hodnocení stupně puchýřkování

ČSN EN ISO 4628-3 (67 3071) (2004), Nátěrové hmoty - Hodnocení degradace nátěrů - Klasifikace množství a velikosti defektů a intenzity jednotných změn vzhledu - Část 3: Hodnocení stupně prorezavění

ČSN EN ISO 4628-4 (67 3071) (2004), Nátěrové hmoty - Hodnocení degradace nátěrů - Klasifikace množství a velikosti defektů a intenzity jednotných změn vzhledu - Část 4: Hodnocení stupně praskání.

ČSN EN ISO 4628-5 (67 3071) (2004), Nátěrové hmoty - Hodnocení degradace nátěrů - Klasifikace množství a velikosti defektů a intenzity jednotných změn vzhledu - Část 5: Hodnocení stupně odlupování.

ČSN EN ISO 4628-8 (67 3071) (2005), Nátěrové hmoty - Hodnocení degradace nátěrů - Klasifikace množství a velikosti defektů a intenzity jednotných změn vzhledu - Část 8: Hodnocení stupně delaminace a koroze v okolí řezu nebo jiného umělého defektu.

ČSN ISO 6270-1 (67 3108) (2002), Nátěrové hmoty – Stanovení odolnosti proti vlhkosti – Část 1: Kontinuální kondenzace.

ČSN ISO 8407 (03 8102) (1995), Koroze kovů a slitin odstranõování korozních zplodin ze vzorků podrobených korozním zkouškám.

Dunne, C.F., Levy, G.K., Hakimi, O. and Aghion, O.E. (2016), "Corrosion behavior of biodegradable magnesium alloys with hydroxyapatite coatings", *Surface and Coatings Technology*, Vol. 289, pp. 37-44.

Gorodylova, N., Dohnalová, Ž., Šulcová, P., Bělina, P. and Vlček, M. (2016), "Influence of synthesis conditions on physicochemical parameters and corrosion inhibiting activity of strontium pyrophosphates $SrM^{II}P_2O_7$ (M^{II} = Mg and Zn)", *Progress in Organic Coatings*, Vol. 93, pp. 77-86.

Graziani, G., Sassoni, E., Franzoni, E. and Scherer, G.W. (2016), "Hydroxyapatite coatings for marble protection. Optimization of calcite covering and acid resistance", *Applied Surface Science*, Vol. 368, pp. 241-257.

Gshalaev, V.S. and Demirchan, A.C. (2013), "Hydroxyapatite: synthesis, properties, and applications", in Chetty, A., Wepener, I., Marei, MK., Kamary, YEl, Moussa, RM (Eds), *Synthesis, Properties, and Applications of Hydroxyapatite*, Nova Biomedical, New York, NY, pp. 91-132.

Hermassi, M., Valderrama, C., Dosta, J., Cortina, J.L. and Batis, N.H. (2015), "Evaluation of hydroxyapatite crystallization in a batch reactor for the valorization of alkaline phosphate concentrates from wastewater treatment plants using calcium chloride", *Chemical Engineering Journal*, Vol. 267, pp. 142-152.

Huang, Y., Hao, M., Nian, X., Qiao, H., Zhang, X., Zhang, X., Song, G., Guo, J., Pang, X. Zhanget. and H, (2016a), "Strontium and copper co-substituted hydroxyapatite-based coatings with improved antibacterial activity and cytocompatibility fabricated by electrodeposition", *Ceramics Inter*, Vol. 42, pp. 260-320.

Huang, Y., Hao, M., Nian, X., Qiao, H., Zhang, X., Zhang, X., Song, G., Zhanget, H. and Shuguang, H. (2016b), "Improving the bioactivity and corrosion resistance properties of electrodeposited hydroxyapatite coating by dual doping of bivalent strontium and manganese ion", *Surface and Coatings Technology*, Vol. 291, pp. 250-215.

Kalita, A. and Kalita, M. (2017), "Williamson-hall analysis and optical properties of small sized ZnO nanocrystals", *Physica. E, Low-Dimensional Systems and Nanostructures*, Vol. 92, pp. 36-40.

Livitska, O., Strutynska, N., Zatovsky, I., Nikolenko, I., Slobodyanik, N., Prylutskyy, Y., Epple, M., Prymak, O. and Byeda, A. (2016), "Copper(II), zinc(II) and copper(II)/zinc (II)-containing carbonate-substituted hydroxyapatite: synthesis, characterization and thermal behaviour", *Materialwissenschaft Und Werkstofftechnik*, Vol. 47 Nos 2/3, pp. 85-91.

Mensah-Darkwa, K., Gupta, R.K. and Kumar, D. (2013), "Mechanical and corrosion properties of magnesium–hydroxyapatite (Mg–HA) composite thin films", *Journal of Materials Science*, Vol. 29, pp. 788-794.

Mojžíš, K. (1967), *Koroze a Ochrana Zařízení v Chemické Výrobě: učební Text Pro Přípravu Dělníků ve Školách Dělnických Povolání, Učební Obory Skupiny Chemie*, 1 vyd., Nakladatelství technické literatury, Praha.

Motevalizadeh, L., Heidary, Z. and Abrishami, M.E. (2014), "Facile template-free hydrothermal synthesis and microstrain measurement of ZnO nanorods", *Bulletin of Materials Science*, Vol. 37 No. 3, pp. 397-405.

Myšková, V. (2014), *Syntéza a Vlastnosti Fosforečnanů Dopovaných Prvky Vzácných Zemin*, Univerzita Pardubice, Pardubice.

Poledno, M. (2003), *Studium Účinnosti Antikorozních Pigmentů na Bázi Fosforečnanů ve Vodou Ředitelných Nátěrových Hmotách*, Univerzita Pardubice, Pardubice. AQ: 4

Přibil, R. (1961), "Komplexometrie", *Státní Nakladatelství Technické Literatury*, Praha.

Reddy, M., Venugopal, A. and Subrahmanyam, M. (2007), "Hydroxyapatite photocatalytic degradation of calmagite (an

azo dye) in aqueous suspension", *Applied Catalysis B: Environmental*, Vol. 69 Nos 3/4, pp. 164-170.

Rivera-Muñoz, E.M. (2011), *Biomedical Engineering - Frontiers and Challenges*, InTech, University Campus STeP Ri.

Šimková, L., Gorodylova, N., Dohnalová, Ž. and Šulcová, P. (2018), "Influence of precipitation conditions on the synthesis of hydroxyapatite", *Ceramics and Silikáty*, Vol. 62, pp. 253-260.

Sommer, L. (1995), "Teoretické základy analytické chemie I", *Vysoké Učení Technické*, Brno.

Záruba, K. (2016), "Analytická chemie", *Vysoká Škola Chemicko-Technologická*, Praha.

Further reading

ČSN 65 4815 (1989), Průmyslová hnojiva. Metody stanovení fosforečnanů.

Corresponding author

Lenka Šimková can be contacted at: st38312@student.upce.cz

AUTHOR QUERIES

AUTHOR PLEASE ANSWER ALL QUERIES

AQau— Please confirm the given-names and surnames are identified properly by the colours.

■=Given-Name, ■= Surname

The colours are for proofing purposes only. The colours will not appear online or in print.

AQ1— To conform to the style guide, please delete the serial comma (comma before "and") from the article title.

AQ2— Please note that the following is unclear as given. Please consider revising for clarity: Surface coating materials that reduced corrosion . . ..

AQ3— Please note that the following is unclear as given. Please consider revising for clarity: For other samples, there is no context between . . ..

AQ4— Kindly provide the issue number for all journal references.